PAPER

Check for updates

Stability of CsPbI₃ with divalent cations incorporated *via* mechanochemical alloying†

Mahsa Shekarnoush, [ID] [ab] Francisco S. Aguirre-Tostado[ac] and Manuel Quevedo López*[a]

Cubic $CsPbI_3$ is a promising perovskite material for optoelectronic applications. This material possesses an energy band gap of 1.7 eV and an optical absorption coefficient of 105 cm^{-1}, and can be synthesized at high temperatures using various methods. However, cubic $CsPbI_3$ faces a significant challenge with degradation reported under ambient conditions. This degradation results in the formation of a delta phase, which comprises a non-perovskite structure with poor optical and electrical properties at room temperature. This paper proposes the partial substitution of lead in $CsPbI_3$ with divalent cations, such as Sn^{2+}, Mn^{2+}, Ni^{2+}, and Ca^{2+}, to improve the overall stability. These cations were selected because their ionic radii meet the Goldschmidt factor and favor the formation of cubic halide perovskites. For the synthesis of the materials, a solid-state mechanochemical method is used that allows for the incorporation of the above-mentioned cations into the $CsPbI_3$ matrix in a single step at room temperature. Replacing Pb^{2+} with Sn^{2+} produced the most stable material and resulted in a cubic perovskite structure with similar optical properties to $CsPbI_3$. In particular, a composition of $CsPb_{0.6}Sn_{0.4}I_3$ resulted in cubic perovskite and did not show degradation when exposed to room temperature, ambient humidity, and atmospheric pressure for up to 25 days. On the other hand, even though Ca^{2+} possesses a smaller ionic radius than Pb^{2+}, replacing Pb^{2+} with Ca^{2+} was not effective in stabilizing $CsPbI_3$ due to the hygroscopic nature of CaI_2. Replacing Pb^{2+} with Mn^{2+} and Ni^{2+} produces stable alloys in a controlled environment (glovebox) at room temperature but quickly decomposes to non-perovskite δ-$CsPbI_3$, iodine, and metal oxides when exposed to air. The degradation mechanism of these materials was studied in detail using XPS techniques, revealing potential alternatives to produce stable Sn^{2+} containing perovskites with properties similar to those of cubic $CsPbI_3$ at room temperature without solvents and increased stability under ambient conditions when Pb^{2+} was partially replaced with Sn^{2+}.

Introduction

Cubic cesium lead iodide ($CsPbI_3$) is a halide perovskite with exceptional optical and electronic properties and has become a promising material for various applications,[1] including solar cells,[2] LEDs,[3] radiation detectors,[4] and photodetectors.[5] With an optimal bandgap of 1.73 eV,[6] $CsPbI_3$ shows efficient absorption of sunlight across a wide range of wavelengths,[7] and its high absorption coefficient in the visible spectrum allows for effective light harvesting.[8] Furthermore, its exceptional charge

carrier mobility facilitates efficient charge transport within the material.[9] Moreover, $CsPbI_3$ exhibits long carrier diffusion lengths, enabling charge carriers to travel significant distances without recombination.[10] Despite its promising properties, $CsPbI_3$ is highly susceptible to degradation processes under ambient conditions that can severely impact its performance and stability.[11] This is primarily due to the fact that, in ABX_3 halide perovskites, A^+ cations typically occupy spaces within the $[BX_3]^-$ framework to ensure structural stability and charge balance[12] but in the case of $CsPbI_3$, the Cs^+ cations are too small to fill the cuboctahedra spaces in the corner-sharing $[PbI_6]^{4-}$ network, which is essential for structural stability.[13]

Preserving the cubic phase structure of $CsPbI_3$ requires a high processing temperature, but as the temperature decreases to room temperature, $CsPbI_3$ tends to degrade.[14] Despite numerous efforts, maintaining a pure cubic phase of $CsPbI_3$ at room temperature remains challenging.[15] Hence, there is a growing interest in developing stable materials with properties

[a] Department of Material Science & Engineering, The University of Texas at Dallas, Richardson, Texas 75080, USA. E-mail: mquevedo@utdallas.edu

[b] Department of Chemistry & Biochemistry, The University of Texas at Dallas, Richardson, Texas 75080, USA

[c] Centro de Investigación en Materiales Avanzados, S. C. (CIMAV), Unidad Monterrey, Apodaca, Nuevo León 66628, Mexico

† Electronic supplementary information (ESI) available. See DOI: https://doi.org/10.1039/d4ma00034j

and structures similar to those of cubic CsPbI$_3$.[16] Several strategies have been explored to increase the stability and performance of CsPbI$_3$-based devices such as chemical passivation techniques,[10] interface engineering,[17] and lattice modification approaches.[18] Chemical passivation involves introduction of moisture-resistant molecules or additives to protect CsPbI$_3$ from moisture-induced degradation.[10] Other alternatives include interface engineering to optimize device architecture and interfaces to prevent moisture penetration and enhance stability.[17] Lattice modification techniques, such as partial substitution of Pb with smaller elements, reduce lattice strain and defects and improve stability.[19] For example, substituting smaller elements on the Pb site can lead to a decrease in lattice strain.[20] Additionally, this process can minimize the formation of defects, ultimately resulting in better resistance against external degradation.[21] This structural stabilization mechanism can effectively suppress phase transitions, lattice distortions, and the formation of non-perovskite phases, thus increasing material stability.

To achieve these effects, the substituting atoms must meet specific criteria. Firstly, a balanced electronic neutrality (or zero charge) must exist between the cations and anions.[22] Secondly, the octahedral factor $(\mu) = R_B/R_X$ should fall within $0.44 \leq \mu \leq 0.9$.[23] This octahedral factor range enables a favorable geometric configuration, leading to the structurally stable perovskite crystal lattice. Lastly, the Goldschmidt tolerance factor (t), defined as $t = (R_A + R_X)\sqrt{2}(R_B + R_X)$, has to be within $0.8 \leq t \leq 1$.[24] In this context, R_A, R_B, and R_X represent the ionic radii of the A, B, and X sites, respectively.[24] The established acceptable range for the tolerance factor (t) in cubic perovskites is $0.9 \leq t \leq 1$.[25] Therefore, selecting elements with appropriate ionic radii and chemical compatibility with the perovskite lattice is crucial for maintaining structural integrity and avoiding phase segregation.

However, transitioning from the theoretical framework to the practical incorporation of alternative elements into the CsPbI$_3$ structures presents its challenges. To incorporate alternative elements into CsPbI$_3$ structures, the standard liquid-based synthesis methods often introduce complex variables like solubility, choice of solvent, stabilizing agents, and temperature control.[26] These factors can significantly affect the final structure and composition of the product.[27] To avoid these issues, alternative synthesis methods to achieve materials that are structurally close to cubic CsPbI$_3$ are currently being investigated. In this regard, ball milling, which is a solid-state technique typically conducted at room temperature, has emerged as a promising alternative.[28] Ball-milling offers a more straightforward and controlled synthesis process, circumventing the complexities associated with liquid-based methods.[29] Although there have been a few studies on synthesizing CsPb$_{1-x}$Sn$_x$I$_3$ using ball milling,[30] this method has rarely been explored for stabilizing CsPbI$_3$ through B-site modification without the use of additives and stabilizing agents under ambient conditions.

In this paper CsPbI$_3$ perovskite materials with divalent cations replacing Pb^{2+} that have optical and structural characteristics like the cubic phase of CsPbI$_3$ at room temperature have been studied. The synthesis is based on a mechanochemical method (ball milling) focusing on substituting lead with elements that have a smaller ionic radius that should produce a perovskite structure with enhanced stability. The proposed method differs from other conventional approaches because it excludes ligands, solvents, or stabilizing agents, without using controlled environment enabling a better evaluation of the chemical reactions involved. Our results identified Sn^{2+} as the most effective element to stabilize CsPbI$_3$ in its solid state and helped understand the degradation mechanisms when Ni^{2+}, Mn^{2+}, and Ca^{2+} are used. The results described a new approach to improving the stability of CsPbI$_3$, specifically replacing "B" site elements using simple mechanochemical methods.

Results and discussion

Tolerance and octahedral factors in the CsMI$_3$ systems (M = Sn^{2+}, Ca^{2+}, Ni^{2+}, and Mn^{2+})

The CsPb$_{1-x}$M$_x$I$_3$ compounds were characterized optically and chemically to investigate the effect of replacing Pb with smaller divalent elements. The divalent cations include Sn^{2+}, Ca^{2+}, Ni^{2+}, and Mn^{2+}, each possessing an ionic radius of 102 pm, 100 pm, 69 pm, and 83 pm, respectively. Fig. 1 shows the relationship between the tolerance and octahedral factors for pure CsMI$_3$ compounds (M = Cd^{2+}, Ca^{2+}, Sn^{2+}, Ni^{2+}, and Mn^{2+}). The mapping reveals an interesting trend: substituting Pb^{2+} with Cd^{2+} and Ca^{2+} results in compounds outside the stability range for cubic perovskites, leading to the formation of orthorhombic structures. Conversely, replacing Pb^{2+} with Sn^{2+}, Ni^{2+}, and Mn^{2+} at specific molar ratios seems to retain the stable cubic perovskite structure range. According to the mapping, Sn^{2+} is the only element that can form a cubic perovskite structure with the formula ABX$_3$. However, a significant challenge arises from
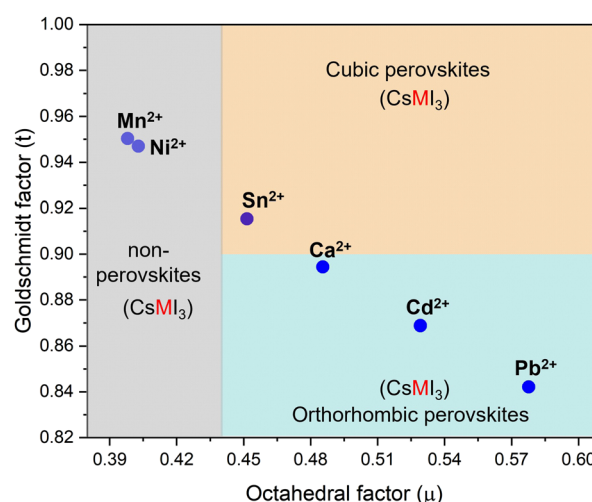

Fig. 1 Calculated tolerance and octahedral factors for CsMI$_3$ perovskites (M = Pb^{2+}, Cd^{2+}, Ca^{2+}, Sn^{2+}, Ni^{2+}, and Mn^{2+}).

the oxidation of Sn^{2+} to Sn^{4+}, posing difficulties in achieving this structure under ambient conditions.

X-ray diffraction analysis

The network of cubic $CsPb_{1-x}Sn_xI_3$ perovskite alloys is composed of Sn(II) and Pb(II) sharing corners, and each surrounded by six halogens forming $[PbI_6]^{4-}$ and $[SnI_6]^{4-}$ units. The cuboctahedra spaces within the structure are occupied by Cs^+ cations.

Fig. 2a shows that the XRD pattern of $CsPb_{1-x}Sn_xI_3$ compounds with a Sn^{2+}/Pb^{2+} molar ratio ranges from 0.05 to 0.5 after a 12-hour ball-milling synthesis. The XRD pattern for the 0.05 molar ratio reveals a dominant peak at 13.02°, corresponding to the (012) plane of δ-CsPbI$_3$. As the molar Sn^{2+}/Pb^{2+} ratio increases to 0.1, an additional peak at 14.46° appears, indicating the presence of the (100) planes for cubic CsPbI$_3$, suggesting the transformation towards the cubic phase. Further increasing the Sn^{2+}/Pb^{2+} molar ratio from 0.1 to 0.4 leads to a considerable reduction in the intensity of δ-CsPbI$_3$ peaks and an increase in the cubic CsPbI$_3$ phase. Remarkably, for a Sn^{2+}/Pb^{2+} molar ratio, the XRD results indicate a pure cubic phase. A slight shift towards higher 2θ degrees is evident in all Sn-containing samples compared to pure CsPbI$_3$, confirming lattice contraction in $CsPb_{1-x}Sn_xI_3$. This is attributed to the incorporation of the smaller Sn^{2+} in the lattice structure.

For a 0.5 Sn^{2+}/Pb^{2+} molar ratio, the orthorhombic CsSnI$_3$ and cubic CsPbI$_3$ phases coexist within the structure. XRD peaks at 14.25°, 25°, and 28.7° confirm orthorhombic CsSnI$_3$, while the peak at 14.46° confirms cubic CsPbI$_3$. This indicates

that a Sn^{2+} molar ratio exceeding 0.4 introduces orthorhombic CsSnI$_3$ into the initially formed cubic crystalline structure. This is a consequence of the excess of Sn^{2+} in the reaction, enabling the formation of the orthorhombic CsSnI$_3$ phase, which has a formation energy lower than cubic CsPbI$_3$ (-1.270 eV per atom for cubic CsPbI$_3$ and -1.203 eV per atom for orthorhombic CsSnI$_3$[31]). These results imply that maintaining a Sn^{2+} ratio below 0.5 is ideal to promote a cubic structure.

The XRD patterns of ball-milled $CsPb_{1-x}Ca_xI_3$ are shown in Fig. 2b. Interestingly, none of the samples showed a cubic phase; instead, all samples exhibited XRD patterns consistent with δ-CsPbI$_3$. This observation is consistent with Fig. 1 where theoretical aspects of cubic perovskites were discussed. In addition to theoretical considerations, the absence of the cubic phase can be attributed to the highly hygroscopic nature of CaI$_2$ within the reaction environment. The presence of the δ-CsPbI$_3$ phase is a consequence of the presence of water in the ambient during the synthesis. The cubic phase cannot be achieved when using Ca^{2+} without using a tightly controlled environment to minimize water during the reaction. These samples were not further analyzed, and the paper focuses on Sn^{2+}, Ni^{2+}, and Mn^{2+}.

Fig. 2c and d show the XRD patterns of $CsPb_{1-x}M_xI_3$, ball-milled for 12 hours, with M representing Ni and Mn, respectively. All XRD patterns are consistent with δ-CsPbI$_3$, with no evidence of the cubic CsPbI$_3$ phase. Upon opening the reaction container, the initial black powder quickly transitioned to yellow within a few minutes. This indicates degradation upon exposure to air. This was explored through XPS,
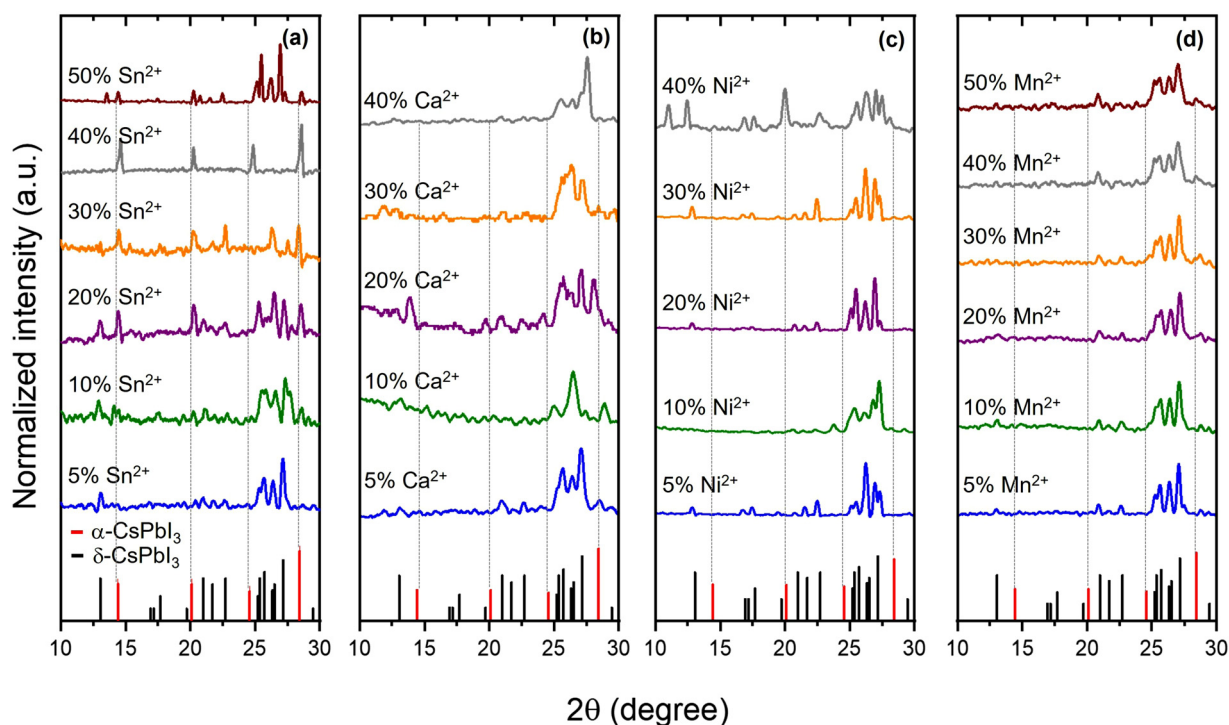

Fig. 2 XRD patterns of 12-h ball-milled $CsPb_{1-x}M_xI_3$ for several M^{2+} atoms, including Sn^{2+} (a), Ca^{2+} (b), Ni^{2+} (c), and Mn^{2+} (d), at various M^{2+}/Pb^{2+} molar ratios.

and a detailed discussion is presented in the following sections.

Stability analysis of CsPb$_{0.6}$Sn$_{0.4}$I$_3$ samples

In terms of phase control and stability the CsPb$_{0.6}$Sn$_{0.4}$I$_3$ is the most promising composition and is analyzed next in detail. Fig. 3 shows the XPS spectra for C 1s, O 1s, Cs 3d, Pb 4f, Sn 3d, and I 3d regions in CsPb$_{0.6}$Sn$_{0.4}$I$_3$ for as prepared samples and those exposed to ambient conditions for 25 days. For clarity, CPSI refers to CsPb$_{0.6}$Sn$_{0.4}$I$_3$.

For both as prepared and 25-day exposed CsPb$_{0.6}$Sn$_{0.4}$I$_3$ samples, the C 1s band shows two distinct chemical components. The first band at 284.8 eV indicates C–C structures commonly associated with surface-adsorbed carbon. The second band, observed at 286.67 eV, is characteristic of carbon in a C–O chemical environment. This latter band is notably enhanced in the samples that have been exposed to ambient conditions for 25 days, suggesting significant interaction with the environment.

Similarly, the O 1s region shows a single chemical environment in both samples, corresponding to oxygen in an OH environment. This feature is likely a result of the samples and precursors being exposed to moisture in the ambient air. The increased OH intensity in the exposed samples compared to the as-prepared samples further supports this conclusion, indicating an interaction with moisture and oxygen in the air.

The Cs 3d region exhibits a doublet at 723.96 eV and 737.90 eV, corresponding to the Cs 3d$_{5/2}$ and Cs 3d$_{3/2}$ states, respectively. These bands confirm the presence of Cs atoms in the CsPb$_{0.6}$Sn$_{0.4}$I$_3$ structure. These bands remain unchanged in both the as-prepared and 25-day exposed samples, indicating the stability of the Cs atoms in the CsPb$_{0.6}$Sn$_{0.4}$I$_3$ perovskites without any significant chemical change.

Similarly, for the Pb 4f region, a doublet is observed at 137.41 eV and 142.30 eV, corresponding to Pb 4f$_{7/2}$ and Pb 4f$_{5/2}$, respectively. This doublet is consistent with the incorporation of Pb atoms in the CsPb$_{0.6}$Sn$_{0.4}$I$_3$ structure and, as in the Cs bands, shows no shift or additional bands in either the as-prepared or the exposed samples, suggesting a stable Pb environment in the CsPb$_{0.6}$Sn$_{0.4}$I$_3$ perovskites.

The Sn 3d region shows a doublet at 485.60 eV and 494.1 eV, associated with Sn 3d$_{5/2}$ and Sn 3d$_{3/2}$, indicative of Sn^{2+} in the CsPb$_{0.6}$Sn$_{0.4}$I$_3$ structure. The stable position of these bands in both the as-prepared and the 25-day exposed samples further supports the chemical stability of Sn^{2+} in the CsPb$_{0.6}$Sn$_{0.4}$I$_3$ perovskites. This observation effectively eliminates concerns regarding the potential oxidation of Sn^{2+} to Sn^{4+} during the synthesis or after ambient exposure.

Lastly, the I 3d region shows a doublet at 618.63 eV and 630.12 eV, corresponding to I 3d$_{5/2}$ and I 3d$_{3/2}$, confirming the presence of iodine. The absence of significant shifts or new bands indicates a stable iodine environment in the CsPb$_{0.6}$Sn$_{0.4}$I$_3$ perovskites.

Fig. 4 illustrates the Kubelka–Munk function derived from UV-vis diffuse reflectance spectra[32] and photoluminescence (PL) spectra of as-prepared CsPb$_{0.6}$Sn$_{0.4}$I$_3$ and 25-day exposed samples.

The Kubelka–Munk function results for both the as-prepared and exposed samples are quite similar, with a bandgap of 1.58 eV. Similarly, the photoluminescence (PL) spectra for both samples show an emission peak at a wavelength ($\lambda_{\max}$) of 794 nm with no significant shift in the emission peak for the sample after 25 days of exposure, suggesting that the optical properties remain stable over time. This consistent optical behavior confirms that the CsPb$_{0.6}$Sn$_{0.4}$I$_3$ sample retains its

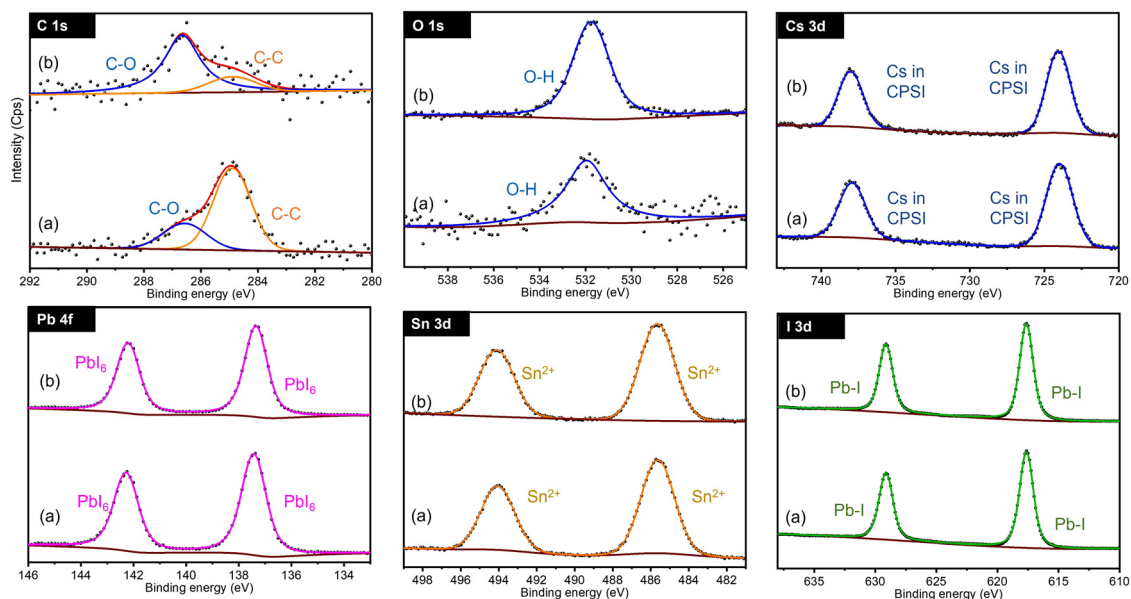**Fig. 3** Comparison of XPS spectra for CsPb$_{0.6}$Sn$_{0.4}$I$_3$ samples at 0 days (a) and after 25 days (b) exposed to ambient conditions. CPSI refers to the CsPb$_{0.6}$Sn$_{0.4}$I$_3$ composition.
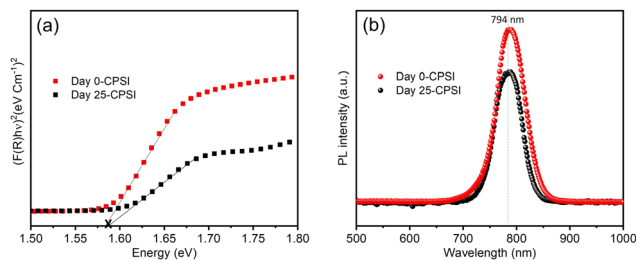
Fig. 4 Kubelka–Munk function (a) and photoluminescence (PL) spectra (b) of $CsPb_{0.6}Sn_{0.4}I_3$ samples as prepared and samples exposed to ambient conditions for 25 days. CPSI refers to the $CsPb_{0.6}Sn_{0.4}I_3$ composition.

inherent characteristics, highlighting its robustness and stability when exposed to ambient conditions for 25 days.

Exploring the degradation mechanisms in $CsPb_{1-x}Ni_xI_3$ and $CsPb_{1-x}Mn_xI_3$ perovskites

$CsPb_{0.9}Ni_{0.1}I_3$. The synthesis of $CsPb_{0.9}Mn_{0.1}I_3$ and 3.3% Ni-doped doped $CsPbI_3$ nanocrystals using solution-based methods at elevated temperatures has been previously reported. These methods also use ligands and stabilizing agents to improve stability and passivation.[33,34] In contrast, our approach explores the stabilization of $CsPbI_3$ by incorporating smaller elements at the B-site using a simple room-temperature solid-state approach. It is worth noting that the mechanochemical synthesis for alloying $CsPbI_3$ with Ni^{2+} and Mn^{2+} used in this paper produces a black powder that, upon exposure to ambient conditions, changed to yellow in a few minutes.

XPS was used to thoroughly investigate the synthesized materials and to study the composition of the as-prepared $CsPb_{0.9}Ni_{0.1}I_3$ samples and monitor compositional changes as a function of exposure time. Two batches of samples were prepared: one in a controlled environment (glove box) and another with exposure to ambient conditions. XPS analyses were conducted in an ultra-high vacuum.

Fig. 5 illustrates the XPS spectra for the C 1s, O 1s, Cs 3d, Pb 4f, Ni 2p, and I 3d regions of the $CsPb_{0.9}Ni_{0.1}I_3$ samples for the controlled and ambient-exposed environments. In the controlled environment, the C 1s region showed distinct binding energies for C in various chemical states - C–C, C–O, and C=O at 284.8 eV, 286.2 eV, and 288.4 eV, respectively. This carbon presence is likely due to residual carbon and oxygen trapped in the precursor cavities during sample preparation. In the ambient-exposed samples, these carbon states were similarly observed.

In the O 1s region, samples from the controlled environment showed a single band indicative of C=O or C–OH bonds, consistent with the C 1s findings. However, in contrast, the samples exposed to air showed additional bands at 529.75 eV and 531.35 eV. These new bands correspond to the formation of nickel oxides, specifically NiO and Ni_2O_3, which indicates significant compositional changes following exposure to air.

The Cs 3d region exhibited a distinctive doublet band with binding energies at 724.5 eV and 738.45 eV, indicative of Cs in the original $CsPb_{0.9}Ni_{0.1}I_3$ perovskite. Also, a new doublet band

is observed at 726 eV and 739.93 eV for the exposed sample, indicating Cs–I formation and confirming a partial decomposition of the perovskites. In contrast, the Pb 4f region showed minimal changes in its binding energies after exposure, implying a limited impact on the chemical environment for Pb^{2+}.

The Ni 2p region showed two initial doublet bands at 855.14 eV and 858.91 eV, associated with Ni^{2+}. Post-exposure, an additional doublet band at 858.80 eV was observed, indicating the oxidation of Ni^{2+} to Ni^{3+}. This finding is consistent with the O 1s region data.

For iodine, both samples exhibited a doublet band at 620 eV and 631.46 eV, corresponding to the I $3d_{5/2}$ and I $3d_{3/2}$ states, signifying iodine integration into the perovskite structure. In air-exposed samples, a new doublet band at 618.75 eV in the I 3d region suggested the presence of an I–I bond.

As explained in the XRD section, exposure of $CsPb_{0.9}Ni_{0.1}I_3$ samples to ambient conditions predominantly led to the formation of the non-perovskite phase δ-$CsPbI_3$. XPS analysis further confirmed the presence of Cs–I, NiO, and Ni_2O_3 in the samples. The XPS and XRD data collectively suggest that $CsPb_{0.9}Ni_{0.1}I_3$ perovskite samples undergo a transformation into non-perovskite forms such as δ-$CsPbI_3$, CsI, NiO, Ni_2O_3, and I_2 when exposed to ambient conditions.

$CsPb_{0.8}Mn_{0.2}I_3$. Fig. 6 shows the XPS spectra for C 1s, O 1s, Cs 3d, Pb 4f, Mn 2p, and I 3d in $CsPb_{0.8}Mn_{0.2}I_3$ for samples in a controlled environment and those exposed to ambient conditions. Bands corresponding to C–C and C–O bonds are observed in both samples, but upon air exposure, an additional band corresponding to C–OOH is observed, suggesting degradation from exposure to the environment.

The O 1s region shows a similar behavior to that in Ni-containing samples. Samples in a controlled environment exhibit a C–OH band, while exposure to air results in two new bands at 530.1 eV and 531.22 eV. These new bands are attributed to the formation of Mn–OH and Mn–O bonds, respectively. This change suggests that the sample undergoes decomposition and reacts with H_2O and O_2 molecules in the air, leading to the formation of these new chemical bonds. This evidence of alteration further underscores the sensitivity of $CsPb_{0.8}Mn_{0.2}I_3$ to ambient conditions and the consequent chemical transformations.

The Cs 3d, Pb 4f, and I 3d regions for $CsPb_{0.8}Mn_{0.2}I_3$ samples show the same behavior as in $CsPb_{0.9}Ni_{0.1}I_3$. This suggests a consistent trend in the chemical states of cesium, lead, and iodine across different perovskite compositions when a portion of lead is substituted by either nickel or manganese.

For the Mn 2p region, the samples in a controlled environment exhibit a doublet band at 642.75 eV, which is characteristic of the Mn^{2+} oxidation state. However, after exposure to air, in addition to the Mn^{2+} bands, a broad band appears at 644.25 eV. This additional band is attributed to MnO, indicating the oxidation of Mn^{2+}. This finding is consistent with the O 1s region, where the appearance of new bands (such as those for Mn–OH and Mn–O bonds) suggests the oxidation of manganese. The correlation between the Mn 2p and O 1s regions in CPMI samples highlights the oxidation of manganese upon
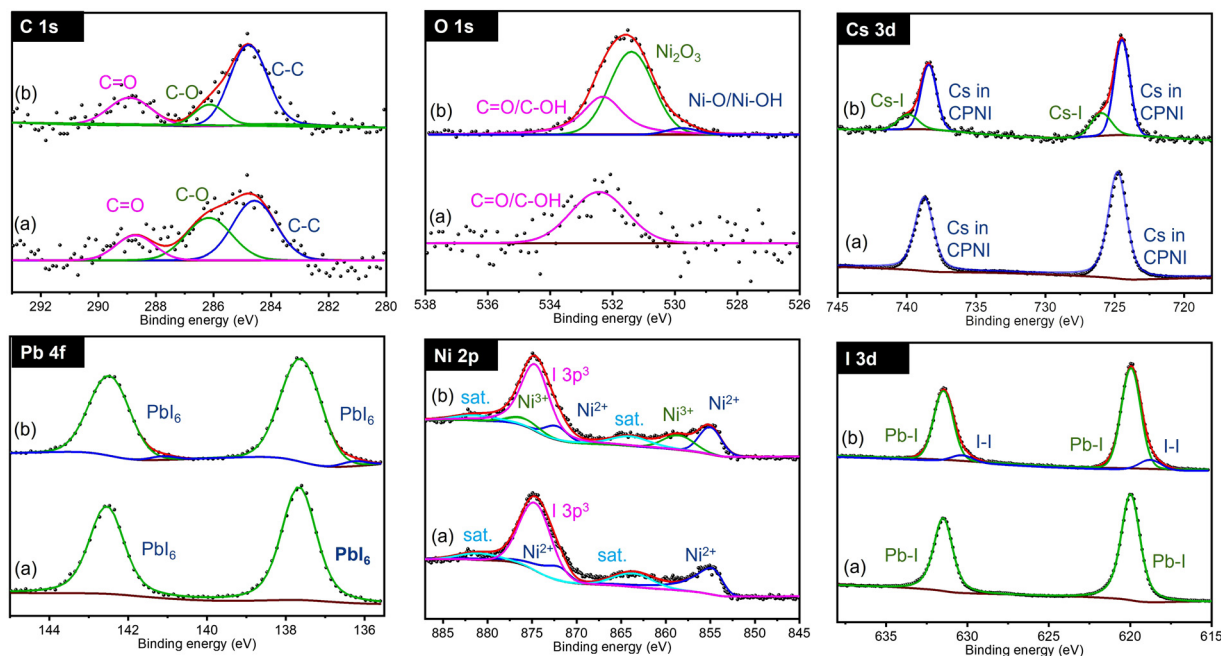
Fig. 5 XPS spectra of $CsPb_{0.9}Ni_{0.1}I_3$ before (a) and after (b) exposure to the ambient conditions, highlighting the C 1s, O 1s, Cs 3d, Pb 4f, Ni 2p, and I 3d regions. CPNI refers to the $CsPb_{0.9}Ni_{0.1}I_3$ composition.
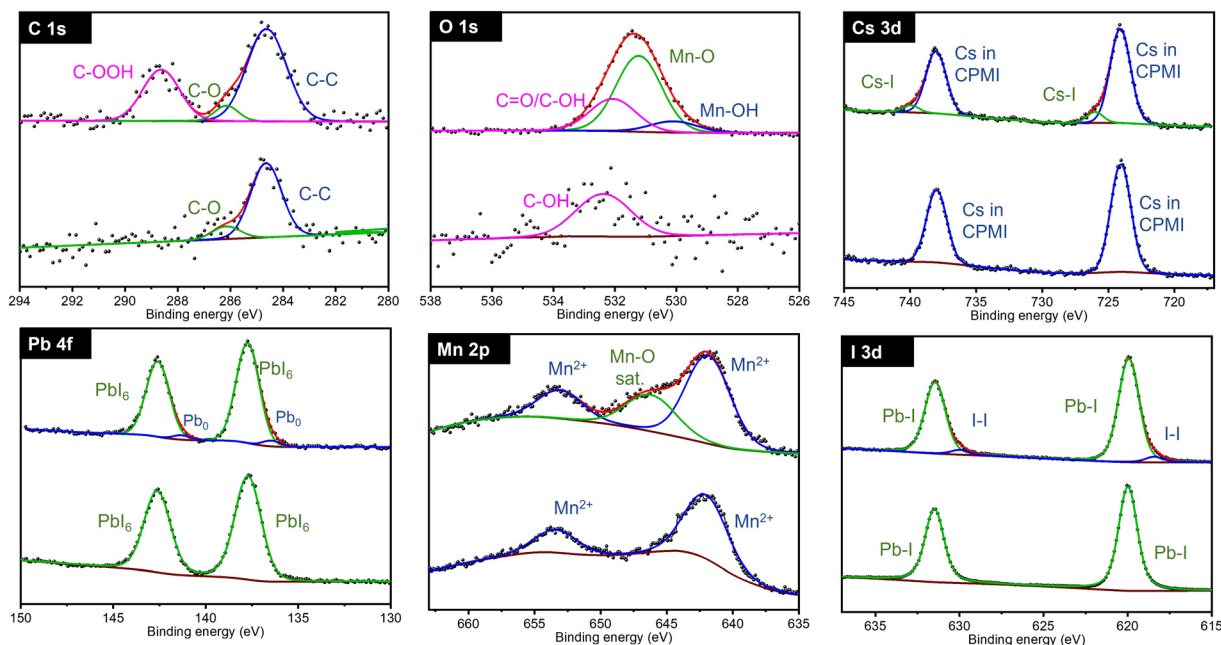

Fig. 6 XPS spectra of $CsPb_{0.8}Mn_{0.2}I_3$ before (a) and after (b) exposure to the ambient conditions, highlighting the C 1s, O 1s, Cs 3d, Pb 4f, Mn 2p, and I 3d regions. CPMI refers to $CsPb_{0.8}Mn_{0.2}I_3$ composition.

exposure to air, underscoring the material's sensitivity to environmental changes.

Degradation mechanism

Fig. 7 shows the proposed degradation mechanism of $CsPb_{0.9}Ni_{0.1}I_3$ and $CsPb_{0.8}Mn_{0.2}I_3$ when exposed to ambient

conditions. The absence of surface passivation in the mechanochemical synthesis used makes both compositions vulnerable to environmental factors such as humidity and oxygen. When exposed to air, the $[NiI_6]^{4-}$ and $[MnI_6]^{4-}$ units in the perovskite network break down, releasing Ni^{2+} and Mn^{2+} ions. These ions then oxidize, forming species such as Ni_2O_3, NiO, $Ni(OH)_2$,
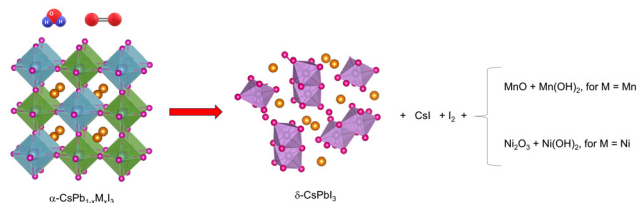
Fig. 7 Proposed degradation mechanism of $CsPb_{0.9}Ni_{0.1}I_3$ and $CsPb_{0.8}Mn_{0.2}I_3$ samples upon exposure to ambient conditions. The Cs, Pb, M (Ni and Mn), and I are colored orange, gray, green, and red, respectively.

MnO, and $Mn(OH)_2$. Furthermore, the decomposition of these perovskites into $[MnI_6]^{4-}$ and $[NiI_6]^{4-}$ also releases I^- ions, which, consequently, form CsI and generate additional I–I bonds.

Ultimately, this degradation leads to the formation of the more stable non-perovskite δ-$CsPbI_3$ phase.

Conclusions

This paper proposes the partial substitution of lead in $CsPbI_3$ with divalent cations, such as Sn^{2+}, Mn^{2+}, Ni^{2+}, and Ca^{2+}, to improve the overall stability. It demonstrates that the stability of $CsPbI_3$ perovskites can be enhanced through mechanochemical alloying and substitution of Pb^{2+} with Sn^{2+} cations. It is shown that Sn^{2+} is particularly effective in stabilizing the cubic phase of $CsPbI_3$ while maintaining its structural integrity and optical properties when exposed to ambient conditions for an extended period. A composition of $CsPb_{0.6}Sn_{0.4}I_3$ results in cubic perovskite and did not show degradation when exposed at room temperature, ambient humidity, and atmospheric pressure for up to 25 days. Although Ca^{2+} possesses a smaller ionic radius than Pb^{2+}, replacing Pb^{2+} with Ca^{2+} is not effective in stabilizing $CsPbI_3$ due to the hygroscopic nature of Ca^{2+}. Materials in which Pb^{2+} is partially replaced with Mn^{2+} and Ni^{2+} are stable in a controlled environment (glovebox) but quickly decompose to non-perovskite δ-$CsPbI_3$, iodine, and metal oxides when exposed to air.

Experimental

Materials

Cesium iodide (CsI, 99.9% trace metal basis), lead(II) iodide (PbI_2, 99.999% trace metal basis), tin(II) iodide (SnI_2, 99.99% trace metal basis), and calcium iodide (CaI_2, 99.5% trace metal basis) were acquired from Sigma Aldrich. Nickel(II) iodide (NiI_2, anhydrous, 99.5%) and manganese(II) iodide (MnI_2, ultra-dry, 99.99%) were purchased from Thermo Fisher Scientific. The stainless-steel balls (10 mm), stainless-steel milling jars, and high energy vertical planetary ball mill used for the solid-state reactions were acquired from MSE Supplies LLC.

$CsM_xPb_{1-x}I_3$ synthesis

For each composition, 2.5 mmol of cesium iodide (CsI) were mixed with (2.5 times (x)) mmol of the MI_2 (MnI_2, NiI_2, CaI_2, and SnI_2) and (2.5 times ($1-x$)) mmol of lead(II) iodide (PbI_2). The mixture was placed in stainless steel jars along with two stainless steel balls. The jars were then inserted into the High Energy Vertical Planetary Ball Milling system, and the samples were collected at different time intervals while maintaining a constant rotation speed of 700 rpm.

Materials characterization

The crystalline structures of the samples were analyzed using a Rigaku SmartLab X-ray diffraction system with a CuK_α radiation source having a wavelength (λ) of 1.5406 Å. XRD measurements were executed at a current of 30 mA and a voltage of 40 kV, with a scan speed set at 3 degrees per minute. X-ray photoelectron spectroscopy (XPS) was employed with a PHI 5000 VersaProbe system for chemical analysis, utilizing a monochromatic Al Ka X-ray source at 1486.7 eV. The XPS spectra were acquired in ultra-high vacuum conditions. AAnalyzer software was employed to analyze the XPS results. UV-vis assessments were conducted using an Agilent UV-vis-NIR system with a multi-angle reflection (R) capability. Photoluminescence (PL) measurements utilized an Ocean Optics QE65000 spectrometer, employing a continuous-wave laser with a wavelength of 405 nm for excitation and a 450 nm long-pass filter.

Author contributions

Mahsa Shekarnoush: conceptualization, formal analysis, methodology, and writing – original draft. Francisco S. Aguirre-Tostado: formal analysis and writing – original draft. Manuel Quevedo-Lopez: conceptualization, funding acquisition, supervision, review and editing.

Conflicts of interest

The authors declare no conflicts of interest.

Acknowledgements

References

1 B. Wang, N. Novendra and A. Navrotsky, Energetics, Structures, and Phase Transitions of Cubic and Orthorhombic Cesium Lead Iodide ($CsPbI_3$) Polymorphs, *J. Am. Chem. Soc.*, 2019, **141**(37), 14501–14504, DOI: 10.1021/jacs.9b05924.

2 J. Wang, Y. Che, Y. Duan, Z. Liu, S. Yang, D. Xu, Z. Fang, X. Lei, Y. Li and S. Liu, Frank). 21.15%-Efficiency and Stable γ-$CsPbI_3$ Perovskite Solar Cells Enabled by an Acyloin

Ligand, *Adv. Mater.*, 2023, **35**(12), 2210223, DOI: **10.1002/adma.202210223**.

3 L.-C. Chen, Y.-T. Chang, C.-H. Tien, Y.-C. Yeh, Z.-L. Tseng, K.-L. Lee and H.-C. Kuo, Red Light-Emitting Diodes with All-Inorganic CsPbI₃/TOPO Composite Nanowires Color Conversion Films, *Nanoscale Res. Lett.*, 2020, **15**(1), 216, DOI: **10.1186/s11671-020-03430-w**.

4 G. Kakavelakis, M. Gedda, A. Panagiotopoulos, E. Kymakis, T. D. Anthopoulos and K. Petridis, Metal Halide Perovskites for High-Energy Radiation Detection, *Adv. Sci.*, 2020, **7**(22), 2002098, DOI: **10.1002/advs.202002098**.

5 M. Afsari, A. Boochani and M. Hantezadeh, Electronic, Optical and Elastic Properties of Cubic Perovskite CsPbI₃: Using First Principles Study, *Optik*, 2016, **127**(23), 11433–11443, DOI: **10.1016/j.ijleo.2016.09.013**.

6 V. A. Saleev and A. V. Shipilova, Ab Initio Modeling of Band Gaps of Cesium Lead Halide Perovskites Depending on the Dopant Amount, *J. Phys.: Conf. Ser.*, 2018, **1096**, 012115, DOI: **10.1088/1742-6596/1096/1/012115**.

7 C. De Weerd, L. Gomez, A. Capretti, D. M. Lebrun, E. Matsubara, J. Lin, M. Ashida, F. C. M. Spoor, L. D. A. Siebbeles, A. J. Houtepen, K. Suenaga, Y. Fujiwara and T. Gregorkiewicz, Efficient Carrier Multiplication in CsPbI₃ Perovskite Nanocrystals, *Nat. Commun.*, 2018, **9**(1), 4199, DOI: **10.1038/s41467-018-06721-0**.

8 M. A. Fadla, B. Bentria, T. Dahame and A. Benghia, First-Principles Investigation on the Stability and Material Properties of All-Inorganic Cesium Lead Iodide Perovskites CsPbI₃ Polymorphs, *Phys. B*, 2020, **585**, 412118, DOI: **10.1016/j.physb.2020.412118**.

9 L.-K. Gao and Y.-L. Tang, Theoretical Study on the Carrier Mobility and Optical Properties of CsPbI₃ by DFT, *ACS Omega*, 2021, **6**(17), 11545–11555, DOI: **10.1021/acsomega.1c00734**.

10 B. Li, Y. Zhang, L. Fu, T. Yu, S. Zhou, L. Zhang and L. Yin, Surface Passivation Engineering Strategy to Fully-Inorganic Cubic CsPbI₃ Perovskites for High-Performance Solar Cells, *Nat. Commun.*, 2018, **9**(1), 1076, DOI: **10.1038/s41467-018-03169-0**.

11 D. Liu, Z. Shao, C. Li, S. Pang, Y. Yan and G. Cui, Structural Properties and Stability of Inorganic CsPbI₃ Perovskites, *Small Struct.*, 2021, **2**(3), 2000089, DOI: **10.1002/sstr.202000089**.

12 A. E. Maughan, A. M. Ganose, A. M. Candia, J. T. Granger, D. O. Scanlon and J. R. Neilson, Anharmonicity and Octahedral Tilting in Hybrid Vacancy-Ordered Double Perovskites, *Chem. Mater.*, 2018, **30**(2), 472–483, DOI: **10.1021/acs.chemmater.7b04516**.

13 J. A. Steele, V. Prakasam, H. Huang, E. Solano, D. Chernyshov, J. Hofkens and M. B. J. Roeffaers, Trojans That Flip the Black Phase: Impurity-Driven Stabilization and Spontaneous Strain Suppression in γ-CsPbI₃ Perovskite, *J. Am. Chem. Soc.*, 2021, **143**(28), 10500–10508, DOI: **10.1021/jacs.1c05046**.

14 R. J. Sutton, M. R. Filip, A. A. Haghighirad, N. Sakai, B. Wenger, F. Giustino and H. J. Snaith, Cubic or Orthorhombic? Revealing the Crystal Structure of Metastable Black-Phase CsPbI₃ by Theory and Experiment, *ACS Energy Lett.*, 2018, **3**(8), 1787–1794, DOI: **10.1021/acsenergylett.8b00672**.

15 B. Ku, B. Koo, W. Kim, Y. Kim, Y.-R. Jeon, M. J. Ko and C. Choi, Room-Temperature Stable CsPbI₃ Perovskite Quantum Dots Prepared by Layer-by-Layer Assembly for Photonic Synapse, *J. Alloys Compd.*, 2023, **960**, 170459, DOI: **10.1016/j.jallcom.2023.170459**.

16 M. Huang, M. Hou, H. Xing, J. Tu and S. Jia, Stable Reconfiguring, High-Density Memory and Synaptic Characteristics in Sn Alloyed CsPbI₃ Perovskite Based Resistive Switching Device, *J. Alloys Compd.*, 2023, **934**, 167719, DOI: **10.1016/j.jallcom.2022.167719**.

17 T. Liu, J. Zhang, M. Qin, X. Wu, F. Li, X. Lu, Z. Zhu and A. K. Y. Jen, Modifying Surface Termination of CsPbI₃ Grain Boundaries by 2D Perovskite Layer for Efficient and Stable Photovoltaics, *Adv. Funct. Mater.*, 2021, **31**, 2009515, DOI: **10.1002/adfm.202009515**.

18 Z. Li, F. Zhou, Q. Wang, L. Ding and Z. Jin, Approaches for Thermodynamically Stabilized CsPbI₃ Solar Cells, *Nano Energy*, 2020, **71**, 104634, DOI: **10.1016/j.nanoen.2020.104634**.

19 Y. Ji, J.-B. Zhang, H.-R. Shen, Z. Su, H. Cui, T. Lan, J.-Q. Wang, Y.-H. Chen, L. Liu, K. Cao, W. Shen and S. Chen, Improving the Stability of α-CsPbI₃ Nanocrystals in Extreme Conditions Facilitated by Mn²⁺ Doping, *ACS Omega*, 2021, **6**(21), 13831–13838, DOI: **10.1021/acsomega.1c01383**.

20 J. L. Teunissen, T. Braeckevelt, I. Skvortsova, J. Guo, B. Pradhan, E. Debroye, M. B. J. Roeffaers, J. Hofkens, S. Van Aert, S. Bals, S. M. J. Rogge and V. Van Speybroeck, Additivity of Atomic Strain Fields as a Tool to Strain-Engineering Phase-Stabilized CsPbI₃ Perovskites, *J. Phys. Chem. C*, 2023, **127**(48), 23400–23411, DOI: **10.1021/acs.jpcc.3c05770**.

21 T. Chen, J. Xie, B. Wen, Q. Yin, R. Lin, S. Zhu and P. Gao, Inhibition of Defect-Induced α-to-δ Phase Transition for Efficient and Stable Formamidinium Perovskite Solar Cells, *Nat. Commun.*, 2023, **14**(1), 6125, DOI: **10.1038/s41467-023-41853-y**.

22 E. A. R. Assirey, Perovskite Synthesis, Properties, and Their Related Biochemical and Industrial Application, *Saudi Pharm. J.*, 2019, **27**(6), 817–829, DOI: **10.1016/j.jsps.2019.05.003**.

23 J. S. Manser, J. A. Christians and P. V. Kamat, Intriguing Optoelectronic Properties of Metal Halide Perovskites, *Chem. Rev.*, 2016, **116**(21), 12956–13008, DOI: **10.1021/acs.chemrev.6b00136**.

24 C. K. Ng, C. Wang and J. J. Jasieniak, Synthetic Evolution of Colloidal Metal Halide Perovskite Nanocrystals, *Langmuir*, 2019, **35**(36), 11609–11628, DOI: **10.1021/acs.langmuir.9b00855**.

25 Z. Qiu, N. Li, Z. Huang, Q. Chen and H. Zhou, Recent Advances in Improving Phase Stability of Perovskite Solar Cells, *Small Methods*, 2020, **4**(5), 1900877, DOI: **10.1002/smtd.201900877**.

26 I. Hwang, Challenges in Controlling the Crystallization Pathways and Kinetics for Highly Reproducible Solution-Processing of Metal Halide Perovskites, *J. Phys. Chem. C*, 2023, **127**(50), 24011–24026, DOI: **10.1021/acs.jpcc.3c05787**.

27 J. Yang, D. K. LaFollette, B. J. Lawrie, A. V. Ievlev, Y. Liu, K. P. Kelley, S. V. Kalinin, J.-P. Correa-Baena and M. Ahmadi, Understanding the Role of Cesium on Chemical Complexity in Methylammonium-Free Metal Halide Perovskites, *Adv. Energy Mater.*, 2023, **13**(33), 2202880, DOI: **10.1002/aenm.202202880**.

28 J.-L. Do and T. Friščić, Mechanochemistry: A Force of Synthesis, *ACS Cent. Sci.*, 2017, **3**(1), 13–19, DOI: **10.1021/acscentsci.6b00277**.

29 C. C. Piras, S. Fernández-Prieto and W. M. D. Borggraeve, Ball Milling: A Green Technology for the Preparation and Functionalisation of Nanocellulose Derivatives, *Nanoscale Adv.*, 2019, **1**(3), 937–947, DOI: **10.1039/C8NA00238J**.

30 Y. El Ajjouri, F. Locardi, M. C. Gélvez-Rueda, M. Prato, M. Sessolo, M. Ferretti, F. C. Grozema, F. Palazon and H. J. Bolink, Mechanochemical Synthesis of Sn (II) and Sn (IV) Iodide Perovskites and Study of Their Structural, Chemical, Thermal, Optical, and Electrical Properties, *Energy Technol.*, 2019, **8**(4), 1900788, DOI: **10.1002/ente.201900788**.

31 *Materials Data on CsSnI3 by Materials Project; mp-568570*, Lawrence Berkeley National Lab. (LBNL), Berkeley, CA (United States), LBNL Materials Project, 2020, DOI: **10.17188/1274524**.

32 S. Landi, I. R. Segundo, E. Freitas, M. Vasilevskiy, J. Carneiro and C. J. Tavares, Use and Misuse of the Kubelka-Munk Function to Obtain the Band Gap Energy from Diffuse Reflectance Measurements, *Solid State Commun.*, 2022, **341**, 114573, DOI: **10.1016/j.ssc.2021.114573**.

33 Q. A. Akkerman, D. Meggiolaro, Z. Dang, F. De Angelis and L. Manna, Fluorescent Alloy CsPbxMn1–xI3 Perovskite Nanocrystals with High Structural and Optical Stability, *ACS Energy Lett.*, 2017, **2**(9), 2183–2186, DOI: **10.1021/acsenergylett.7b00707**.

34 M. Liu, N. Jiang, H. Huang, J. Lin, F. Huang, Y. Zheng and D. Chen, Ni2 + -Doped CsPbI3 Perovskite Nanocrystals with near-Unity Photoluminescence Quantum Yield and Superior Structure Stability for Red Light-Emitting Devices, *Chem. Eng. J.*, 2021, **413**, 127547, DOI: **10.1016/j.cej.2020.127547**.